Available online at www.sciencedirect.com
ScienceDirect
International Journal of Heat and Fluid Flow 28 (2007) 63–71
International Journal of HEAT AND FLUID FLOW
www.elsevier.com/locate/ijhff

Experimental investigation of R-134a and R-245fa two-phase flow in microchannels for different flow conditions

Rémi Revellin *, John R. Thome

Heat and Mass Transfer Laboratory, Ecole Polytechnique Fédérale de Lausanne (EPFL), CH-1015 Lausanne, Switzerland

Accepted 3 May 2006
Available online 22 August 2006

Abstract

An optical measurement method for two-phase flow characterization in microtubes has been applied to determine the frequency of bubbles exiting a microevaporator, the coalescence rates of these bubbles and their lengths as well as their mean two-phase vapor velocity. The tests were run in 0.5 mm and 0.8 mm diameter glass channels using R-134a and R-245fa at 26, 30 and 35 °C saturation temperatures. Four flow patterns (bubbly flow, slug flow, semi-annular flow and annular flow) with their transitions (bubbly/slug flow and slug/semi-annular flow) were detected. The two-phase flow pattern transitions observed with R-134a did not compare well to a leading macroscale flow map for refrigerants nor to a microscale map for air–water flows. No significant influence of the inlet subcooling (2, 3, 5 °C) nor the saturation pressure has been observed on the flow pattern transitions. Furthermore, changing the heated length from 70 to 30 mm before the glass tube did not influence the location of the transition lines in the flow pattern map. The 0.8 mm diameter also did not show any significant difference to the 0.5 mm channel, although bubbly/slug flow was present over a wider range of mass flux. The transitions between flow regimes are less influenced by the mass flux for R-245fa than for R-134a; thus for low mass fluxes the difference is significant and the flow regimes appear earlier in terms of vapor quality.

Keywords: Flow patterns; Microchannels; Two-phase flow

1. Introduction

In the interest of providing higher cooling capability for microtechnologies, the fundamentals of two-phase heat transfer in microchannels are being studied ever more extensively. Many two-phase flow and heat transfer prediction methods exist for vaporization inside macrochannels but these are not suitable to use for microchannels due to small-scale phenomena. Therefore, research is underway to investigate these small-scale phenomena and characterize the two-phase flow process. The most important parameters controlling two-phase flow in microchannels are bubble frequencies, lengths and velocities, coalescence of bubbles and flow pattern transitions. These were measured and/or detected by an optical measurement technique developed specifically for this purpose, only the results for the velocities and the flow patterns are presented here.

To better predict heat transfer coefficients in microcooling elements and heat spreaders for electronic cooling, for example, it is desirable to develop a flow pattern map for predicting the flow regimes of two-phase flow in microchannels. Due to the predominance of surface tension over gravity forces, the tube orientation has negligible influence on the flow pattern. For this reason, in horizontal microchannels stratified flow (as verified by Triplett et al. (1999); Damianides and Westwater (1988) and Serizawa et al. (2002)) does not exist. Slug flow also occupies a much larger range of vapor qualities when compared with large diameter channels (Wambsganss et al., 1993).

Among the first studies to describe flow patterns in microchannels is that by Suo and Griffith (1964). They denoted three different flow patterns in their study using channels of 0.514–0.795 mm: bubbly/slug, slug and annular flow. Similarly, the study of Cornwell and Kew (1992) also

* Corresponding author. Tel.: +41 0 21 693 54 35.
E-mail address: remi.revellin@epfl.ch (R. Revellin).

0142-727X/$ - see front matter © 2006 Elsevier Inc. All rights reserved.
doi:10.1016/j.ijheatfluidflow.2006.05.009

Nomenclature

Greek letters

δ	liquid film thickness, m
ΔT_{sub}	subcooling of liquid, °C
ρ	density, kg m^{-3}

Latin letters

a	Garimella et al. parameter, kg m^{-2} s^{-1}
b	Garimella et al. parameter, kg m^{-2} s^{-1}
D	tube diameter, m
D_1	tube diameter in Garimella et al. Equation, mm
G	mass flux, kg m^{-2} s^{-1}
J	superficial velocity, m s^{-1}
L	length, m
P	pressure, bar
q	heat flux, kW m^{-2}
R	internal radius of the tube, m
T	temperature, °C
U	velocity, m s^{-1}
x	vapor quality, %

Subscripts

dry	dryout zone
film	liquid film between the bubble and the wall
Hom	from homogeneous model
l	liquid
out	outlet
p	pair (liquid slug/bubble)
sat	saturation
sub	subcooling
total	total
v	vapor
0	initial

found three different flow patterns in rectangular channels (1.2×0.9 mm and 3.5×1.1 mm): isolated bubbles, confined bubbles, and slug/annular flow. Since then, many others have observed these three basic flow patterns: Sheng and Palm (2001) for 1–4 mm tubes, Damianides and Westwater (1988) for a 1 mm tube, Mertz et al. (1996) and Kasza et al. (1997) for a single rectangular channel of 2.5 mm by 6 mm, and Lin et al. (1998) using a single round tube of 2.1 mm inside diameter. Yun and Kim (2004) studied two-phase flow regimes of CO_2 in a narrow rectangular channel having a width of 16 mm and a height of 2 mm. They denoted only three different flow patterns: Bubbly flow, Intermittent flow and Annular flow.

Some other authors describe microchannel two-phase flow using additional flow pattern designations, such as Triplett et al. (1999) using both rectangular and circular channels or Steinke et al. (2003) who found no difference in the theory used for macroscale channels. Yang and Shieh (2001) concluded their study on flow patterns of air–water and two-phase R-134a in small circular tubes by saying that none of the existing flow pattern maps were able to predict air–water and refrigerant flow pattern transitions in small tubes. Serizawa et al. (2002) observed several distinctive flow patterns using air–water and steam-water flow in very small circular tubes of 20, 25, 50 and 100 μm diameter: dispersed bubbly flow, gas slug flow, liquid ring flow, liquid lump flow, annular flow, frothy or whispy annular flow, rivulet flow and liquid droplet flow. Saitoh et al. (2005) experimentally investigated the boiling heat transfer of R-134a in horizontal small-diameter tubes with inner diameter of 0.51, 1.12 and 3.1 mm. They found that the flow inside the tube approached homogeneous flow when decreasing the tube diameter. They also found four different flow patterns: Plug flow, Slug flow, Wavy-annular flow and Annular flow. Garimella et al. (2002) proposed a correlation for flow transition during condensation of R-134a in circular channels (0.5 to 4.91 mm) with the hydraulic diameter (in mm) as parameter to determine the transition between intermittent and non-intermittent flow as shown in Eq. (1).

$$x = \frac{a}{G + b} \tag{1}$$

with

$$a = 69.5673 + 22.595 \exp(0.2586 D_1) \tag{2}$$

$$b = -59.9899 + 176.8137 \exp(0.3826 D_1) \tag{3}$$

The difficulty of identifying flow regimes and their transitions comes from the difficulties in obtaining good high speed images, in the interpretation of the flow (subjectivity and pattern definition depending on the author), and also in choosing the channel size that determines either macro or microscale or the transition between them.

Thome et al. proposed the first mechanistic heat transfer model to describe evaporation in microchannels with a *three-zone* flow boiling model that describes the transient variation in the local heat transfer coefficient during sequential and cyclic passage of (i) a liquid slug, (ii) an evaporating elongated bubble, and (iii) a vapor slug when film dryout has occurred. Fig. 1 depicts a schematic of their three-zone heat transfer model. The new model illustrates the strong dependency of heat transfer on the bubble frequency, the lengths of the bubbles and liquid slugs and the liquid film thickness and is so far only applicable to the slug flow regime.

For these reasons, it is opportunistic to apply an optical measurement technique to quantitatively characterize flow pattern transitions and to measure the frequency, velocity and length of vapor bubbles in microchannels, in particular at the exit of microevaporators in which the flows are

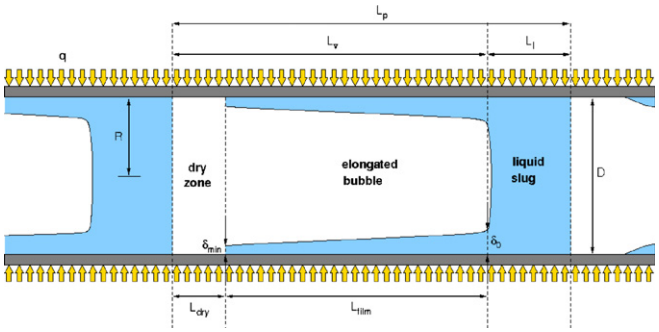

Fig. 1. Schematic of three-zone evaporation model.

formed. Such an optical measurement technique has been developed here and implemented in a new multi-purpose microchannel test facility and is presented in this article together with the new results.

2. Description of the test facility

A new experimental stand was built in order to control the fluid characteristics at the inlet of the test section, i.e. mass flow rate, inlet subcooling and saturation pressure. The test facility is shown in Fig. 2 and was designed with two optional methods for controlling the flow through the heat transfer and flow visualization test sections: (i) using a speed controlled micropump (*Pump mode*), and (ii) using the pressure difference between the upstream temperature-controlled refrigerant storage vessel (called also the hot reservoir) and its downstream companion (called also the cold reservoir) (*Reservoir mode*). A Labview interface has been created to control its operation and register measurements. A valve has been installed between the hot reservoir and the test section to avoid oscillations when boiling starts in the test section by increasing the pressure drop in the loop, so that back flow can be suppressed and a wider range of stable operations conditions achieved.

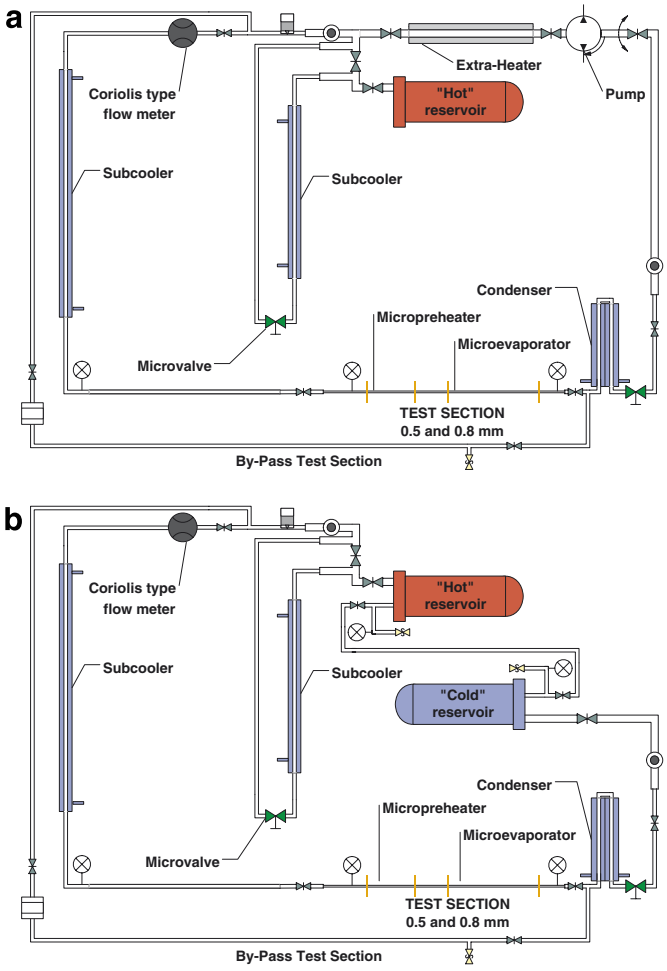

Fig. 2. Schematic of (a) pump loop and (b) reservoir loop.

2.1. Test section

The test section consisted of an 80 mm long stainless steel tube used as a preheater, a 20 mm long glass tube for electrical insulation, a 110 mm long stainless steel tube heated section as the microevaporator and then a 100 mm long glass tube for flow pattern visualization and optical measurements, as shown in Fig. 3. The internal diameters of all these sections were 0.50 mm and 0.80 mm. Two copper clamps were attached to the preheater and to the evaporator. They were connected electrically to two Sorensen power supplies that delivered direct current and heated the tubes by Joule effect. The vapor quality entering the flow visualization tube was calculated from an energy balance from the Joule heating at the outlet of the evaporator tube just before the glass visualization tube. Two pressure transducers were installed at the inlet and outlet of the test section as shown in Fig. 2 where the inside diameter is 4 mm. Two 0.25 mm thermocouples were placed in the fluid at the same locations. Four 0.25 mm thermocouples were also attached on the external surface of the microtubes in an adiabatic location (before the inlet and after the outlet of both the preheater and the evaporator) to measure fluid temperature. Two more 0.25 mm thermocouples were installed on the two heated tubes to avoid dry out and overheating. All the test section was thermally insulated.

It is of particular importance here to note that the present setup concerns actual two-phase flows exiting a microevaporator channel and not two-phase flows generated by a gas injector or liquid-vapor mixer. Hence, the bubbles

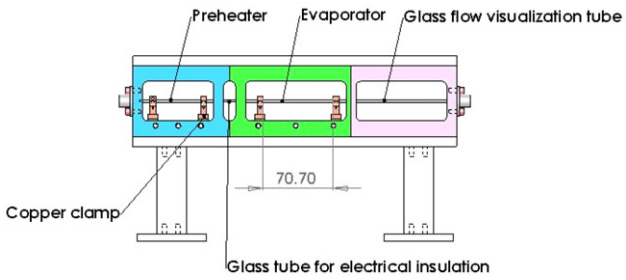

Fig. 3. Schematic diagram of the test section: front view.

and subsequent flow regimes observed here originated from nucleation in the evaporator and then further evaporation during the flow downstream, just like in a microchannel cooling element attached to a computer chip, for instance. Thus, here the resulting flow pattern and bubble characteristics are determined by the process itself, not imposed or influenced by the design of the injector or mixer.

2.2. Experimental conditions and uncertainties

The experimental conditions are summarized in Table 1. Prior to the tests, energy balances were carried out on the test section for subcooled flow of R-134a. The difference in the energy balances between the liquid and the Joule heating diminished to within 2–3% for the maximum heat duties feasible for subcooled conditions, which are at the low end of heat duties for the evaporation tests. Hence, the energy balances (and the direct effect on local vapor qualities) are thought at worst to be ±2–3% but are probably ±1% for most of the two-phase conditions cited in Table 1.

When running two-phase experiments, the refrigerant arrives at the inlet of the preheater as a subcooled liquid. Then, it is heated to the desired temperature and enters into the evaporator to be partially evaporated. For the present tests, the reservoir mode was always used for driving the refrigerant as this gave the most stable flow.

A Coriolis mass flow meter was used to measure the flow rate of the subcooled R-134a or R-245fa to an accuracy of ±1% of the reading. The Joule heating was obtained by measuring the dc voltage to an accuracy of ±0.02% and the dc current by a dc current transformer with an accuracy of ±3.5% for low currents and ±1% for high values. The absolute pressure transducers for monitoring the local pressures were accurate to ±5 mbar. Thermocouples were accurate to ±0.1 °C according to their calibrations. The vapor quality entering the flow visualization tube was estimated to be accurate to ±2% for most test conditions. The pressure drops in the visualization tube reached up to 1.2 bar (the pressure drops were obtained from the measured differences in saturation temperature between the inlet and outlet of the visualization tube); this phenomena leads to an increase of the vapor quality along the tube from a flashing effect. The vapor velocity is by consequence increased due to this change of vapor quality. This variation of the vapor velocity is taken into account when processing the data.

Table 1
Experimental conditions

Parameter	Range	Units
Fluid	R-134a, R-245fa	–
D	0.50, 0.80	mm
L(heated)	70, 50, 30	mm
G	200–2000	kg m^{-2} s^{-1}
q	3.2–422.1	kW m^{-2}
T_{sat}	26, 30, 35	°C
ΔT_{sub}	2, 3, 5	°C
x_{out}	0.1–95.4	%

3. Optical measurement technique

An optical method to count bubbles and determine the two-phase flow characteristics has been used. The experimental setup consisted of two laser beams, with a power less than 1 mW, directed through the glass visualization tube and the fluid inside at two different locations, separated by a distance of 70.63 mm as presented in Fig. 4. Two lenses focused the laser beams to the middle of the microtube. Two photodiodes on the opposite side of the microtube, their faces painted over but leaving only a vertical 1 mm wide opening in the middle to isolate the signal, measured the intensity of the light. They were connected to a *National Instruments* SCXI acquisition system using a scan rate of 10 000 measurements/s to measure the resulting voltage signals from the two diodes. A micropositioning system was used to align the laser beams with the lenses and photodiodes. The laser beams interact locally with the structure of the flow and by signal processing, it was possible to determine the velocity, length and frequency of vapor bubbles. The signals from the diodes obtained by this technique for the different flow regimes are similar to those obtained by Lowe and Rezkallah (1999) using a void fraction probe for a microgravity air/water two-phase flow in a 9.525 mm tube.

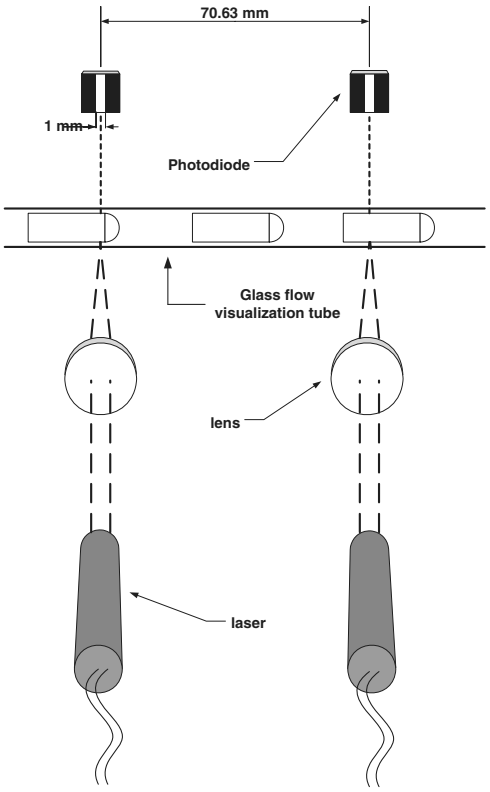

Fig. 4. Schematic diagram of the laser instrumentation.

The signal processing of our optical measurements consisted of several steps and is detailed in Revellin et al. (2006).

4. Experimental results

4.1. Vapor bubble velocities

Fig. 5 shows vapor bubble velocities from laser 2 plotted versus the thermodynamic vapor quality at that location. Here, mean velocities calculated from the homogeneous void fraction equation have also been plotted from the following expression:

$$U_{\mathrm{Hom}} = G_{\mathrm{total}}\left[\frac{x}{\rho_{\mathrm{v}}} + \frac{1-x}{\rho_{\mathrm{l}}}\right] \tag{4}$$

In general, the qualitative comparison shows that the vapor velocity is close to that of homogeneous flow at low vapor qualities and deviates from this model at higher vapor qualities. The vapor velocity is close to homogeneous for small vapor bubbles or small elongated bubbles. Due to the velocity profile in the boundary layer the vapor bubbles near the wall are deformed as can be observed in the video images shown in the next section. Furthermore, the channel is horizontal and hence there is no buoyancy effect to lift the bubble as in slug flows in vertical channels.

4.2. Flow patterns

Four principal flow patterns and two intermediate transition regimes have been observed in the present study.

The microscale flow patterns observed are defined as follows:

Bubbly flow:

In bubbly flow, the vapor phase is distributed as discrete bubbles in a continuous liquid phase and the bubbles are smaller in length than the diameter of the tube. This flow pattern covers a very small range of vapor quality and is more or less nonexistent at high mass flux. It is of importance to note that the influence of heat flux is not studied here, only the influence of vapor quality at the outlet of the heated microtube. Fig. 6(a) shows a picture taken with a high definition video camera.

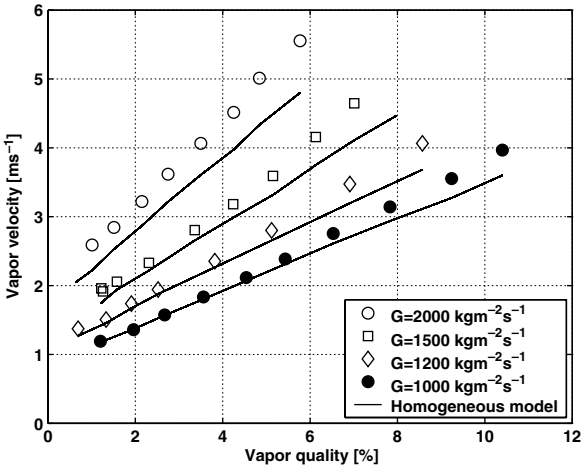

Fig. 5. Vapor velocity versus vapor quality from laser 2 for R-134a, $D = 0.5$ mm, $L = 70.70$ mm, $T_{\mathrm{sat}} = 30$ °C, $\Delta T_{\mathrm{sub}} = 3$ °C at inlet to evaporator for slug and slug/semi-annular flows.

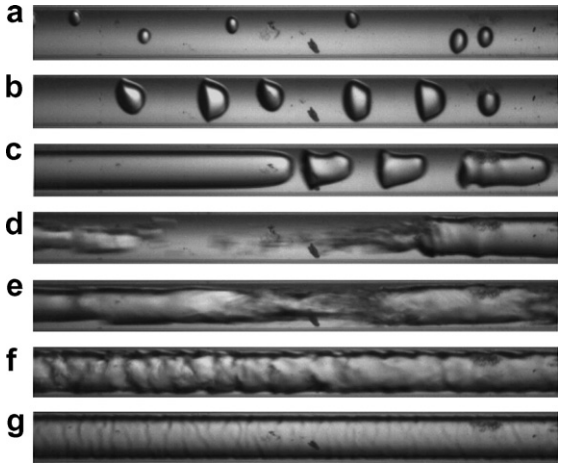

Fig. 6. Flow patterns and transitions for R-245fa, $D = 0.5$ mm, $L = 70.70$ mm, $G = 500$ kg m^{-2}s^{-1} and $T_{\mathrm{sat}} = 35$ °C. (a) Bubbly flow at $x = 3.8\%$. (b) Bubbly/slug flow at $x = 4\%$. (c) Slug flow at $x = 4.3\%$. (d) Slug/semi-annular flow at $x = 7.6\%$. (e) Semi-annular flow at $x = 15\%$. (f) Wavy annular flow at $x = 23\%$. (g) Smooth annular flow at $x = 23\%$.

Bubbly/slug flow:

In bubbly/slug flow, bubbly flow (described above) and slug flow (described below) are both present. Fig. 6(b) shows a picture taken with a high definition video camera. The count rates increases rapidly with the heat flux in the evaporator, reaches a peak and then decreases due to coalescence of small and elongated bubbles.

Slug flow:

In slug flow, the vapor bubbles are approximately the same diameter as the tube. The nose of the bubble has a characteristic hemispherical cap and the vapor in the bubbles is separated from the tube wall by a thin film of liquid. The liquid flow is contained mostly in the liquid slugs which separate successive vapor bubbles. The length of the vapor bubbles can vary considerably. Fig. 6(c) shows a picture taken with a high definition video camera. The count rates decrease with increasing vapor quality due to coalescence of elongated bubbles.

Slug/semi-annular flow:

In slug/semi-annular flow, the slug (described above) and semi-annular (described below) flows are both present. The vapor velocity increases with heat flux and the rear of elongated bubbles are more and more deformed, (see Fig. 6(d)) as shear forces are more and more important. When coalescence occurs, transitions are no longer clean but instead create a churn-like zone where the liquid slug was.

Semi-annular flow:

In semi-annular flow, liquid slugs are nonexistent as shown in Fig. 6(e). A liquid film forms at the tube wall with a continuous central vapor core. It is separated by churning liquid zones due to the previous deformation of the rear ends of elongated bubbles and the coalescence of bubbles. Limits of this transition are the end of slug/semi-annular flow and the beginning of annular flow. It is interesting to emphasize that the churning liquid disappears gradually from the beginning of this transition up to the end.

Annular flow:

In annular flow, a liquid film flows on the tube wall with a continuous central vapor core. It is the same definition as for semi-annular flow, except that the churning liquid zones do not exist anymore. Annular flow is characterized by two types of annular flow: wavy and smooth, where the wavy annular flow signals have a small scale fluctuation from the waves on the annular film. These two types of annular flow can be seen in Fig. 6(f) and (g).

Two-phase flow pattern observations based on the present observations with the two laser signals are presented in Fig. 7 in mass flux versus vapor quality and superficial liquid velocity versus superficial vapor velocity formats, which are calculated from the test results as follows:

$$J_l = \frac{(1-x)G}{\rho_l} \tag{5}$$

$$J_v = \frac{xG}{\rho_v} \tag{6}$$

Notably, the higher the mass flux, the earlier annular flow is reached. Bubbly flow is more or less nonexistent for mass fluxes greater than 1000 kg m^{-2} s^{-1}. The most important observation to make about the flow patterns in the present study is that their transitions are controlled primarily by the rate of coalescence as shown in Revellin et al. (2006), which is not recognized as a contributing factor by any of the microscale (nor macroscale) flow pattern maps.

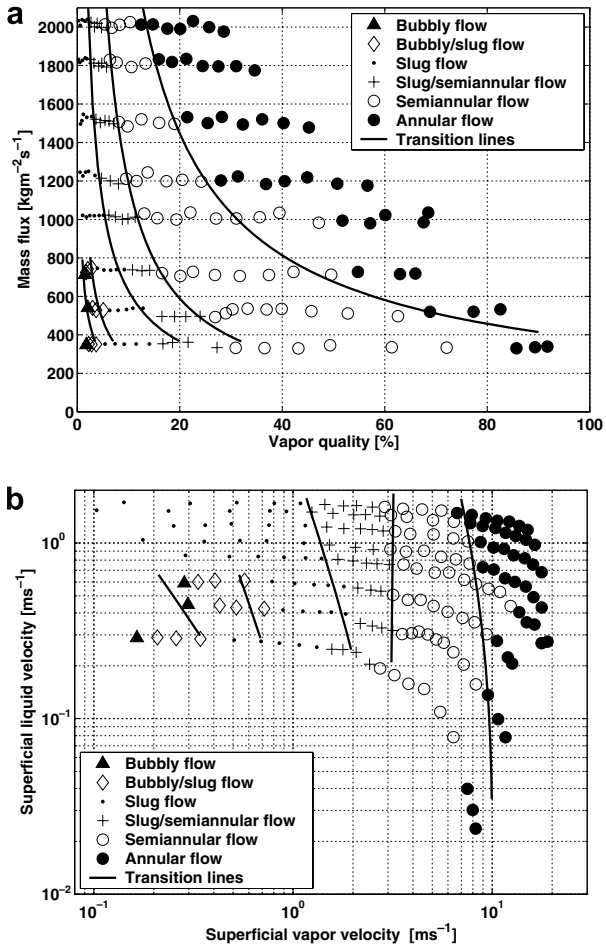

Fig. 7. Flow pattern maps with experimental transition lines for R-134a, $D = 0.5$ mm, $L = 70.70$ mm, $T_{sat} = 35$ °C, $\Delta T_{sub} = 5$ °C using laser 1. (a) Flow pattern observations from laser 1 with transition lines. (b) Flow pattern map from laser 1 with transition lines.

4.3. Flow pattern maps

A comparison with the macroscale map of Kattan et al. (1998) for refrigerants shows a significant difference in the transition line locations and also the flow patterns encountered (Fig. 8(a)), illustrating that the current observations cannot be classified as macroscale two-phase flows. Fig. 8(b) shows a comparison between the present experimental transition lines from laser 1 and those of Triplett et al. (1999) available for air/water flow in a 1.097 mm tube diameter; the results are not in good agreement when extrapolating their air–water map to R-134a.

Fig. 9 presents transition lines for three different inlet subcoolings: 2, 3 and 5 °C. It shows no significant effect of this parameter on the transition lines. No bubbly flow has been observed for $\Delta T_{sub} = 2$ and 3 °C but it would probably have been seen at the lower mass fluxes but the tests could not be run at those conditions due to instabilities. Hypothetically, a larger inlet subcooling would reduce the two-phase zone in the microevaporator that would result in smaller bubbles at the outlet of the heated tube at a given mass flux and vapor quality. The transitions between flow regimes would probably appear later in terms of vapor quality.

The effect of the saturation temperature is shown in Fig. 10 for tests at inlet saturation temperatures of 26, 30 and 35 °C (6.9, 7.7 and 8.9 bar saturation pressures). No bubbly flow has been observed for $T_{sat} = 35$ °C for the same reason explained in the previous paragraph. No significant difference in the location of the transition lines have been observed except for the semi-annular/annular transition. For $T_{sat} = 30$ °C, the transition appears earlier, which is not consistent with the two others. This transition is more difficult to specify than the others as it is directly dependent on the threshold position. Furthermore, it is probably appropriate to talk about transition "zones" or "regions" instead of "lines". The dashed line corresponds to the transition of Garimella et al. (2002) given by Eq.

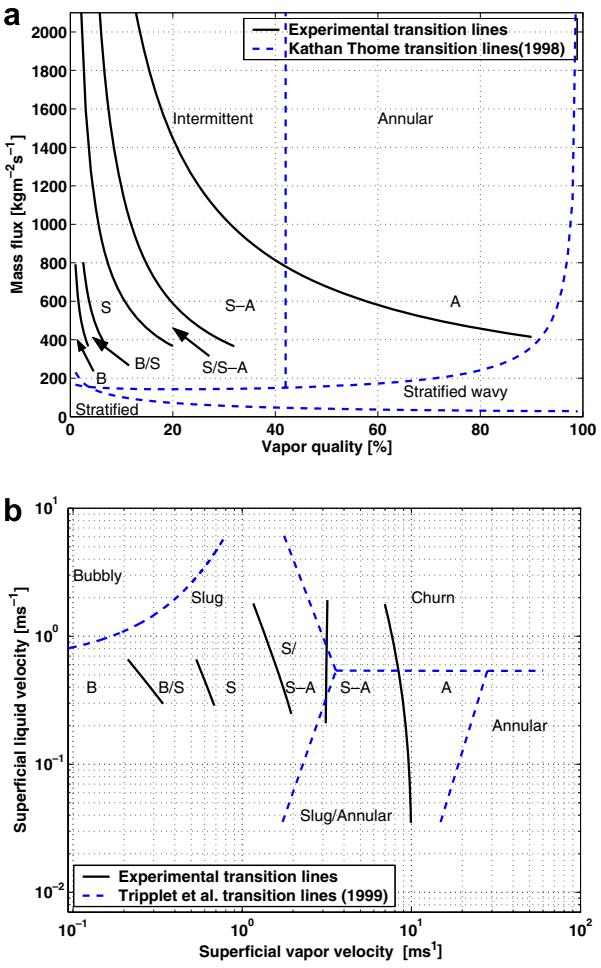

Fig. 8. Comparison between present flow pattern transition observations for R-134a, $D = 0.5$ mm, $L = 70.70$ mm, $T_{sat} = 30$ °C, $\Delta T_{sub} = 3$ °C and two different flow pattern maps available for macro and micro-scale. (a) Comparison between present experimental transition lines from laser 1 and Kattan-Thome-Favrat macroscale map in a mass flux versus vapor quality format for R-134a, $D = 0.5$ mm, $L = 70.70$ mm, $T_{sat} = 30$ °C, $\Delta T_{sub} = 3$ °C. *(B = Bubbly flow, B/S = Bubbly/slug flow, S = Slug flow, S/S-A = Slug/semi-annular flow, S-A = Semi-annular flow, A = Annular flow)*. (b) Comparison between present experimental transition lines from laser 1 and Triplett et al. transition lines available for air–water flow in a 1.097 mm tube diameter.

(1), the latter of which is a natural occurrence during condensation of saturated vapor. Their equation is available for condensation of R-134a and determines the transition between intermittent and non-intermittent flow. As can be seen, the Garimella et al. (2002) transition is close to that between slug/semi-annular and semi-annular flow observed in the present study, especially at high mass flux, giving a similar trend. The coalescence process will obviously be different in an evaporating process compared to the break down of bubbles in a condensing one.

Fig. 11 presents the influence of the heated length on the transitions between the different flow regimes. No significant difference in the location of the transition lines have been observed excepted for the semi-annular/annular transition. For $L = 50$ mm, the transition appears to be inconsistent with the two other transitions, for the same reasons

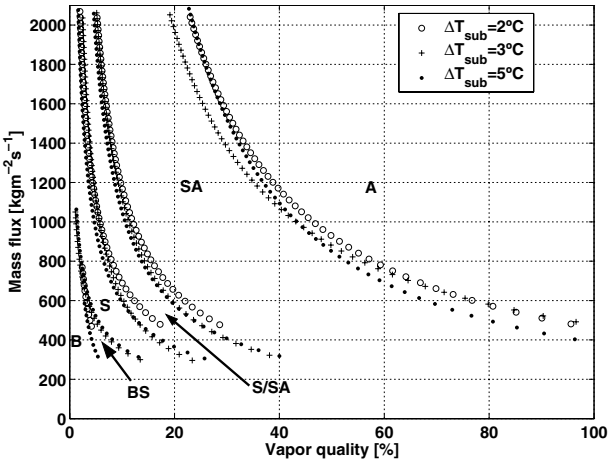

Fig. 9. Comparison between experimental transition lines from three different inlet subcooling at inlet to evaporator from laser 1 for R-134a, $D = 0.5$ mm, $L = 70.70$ mm, $T_{sat} = 35$ °C.

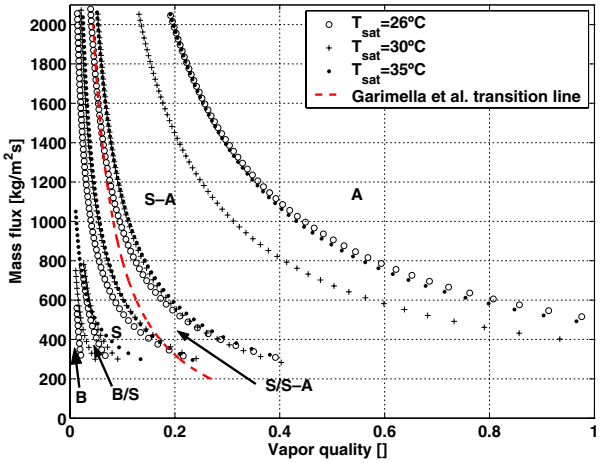

Fig. 10. Comparison between experimental transition lines from three different saturation temperatures from laser 1 for R-134a, $D = 0.5$ mm, $L = 70.70$ mm, $\Delta T_{sub} = 3$ °C.

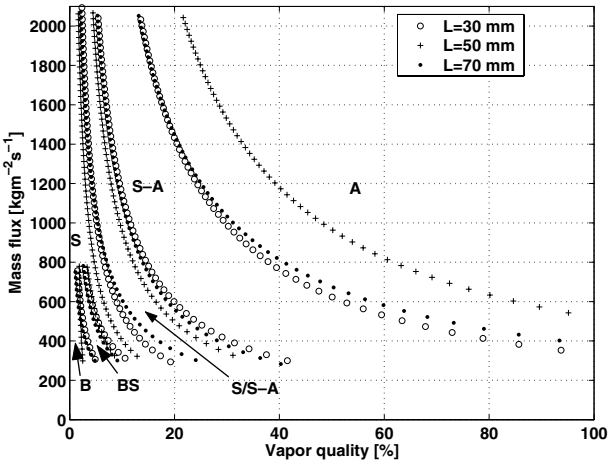

Fig. 11. Comparison between experimental transition lines from three different heated lengths from laser 1 for R-134a, $D = 0.5$ mm, $\Delta T_{sub} = 3$ °C, $T_{sat} = 30$ °C.

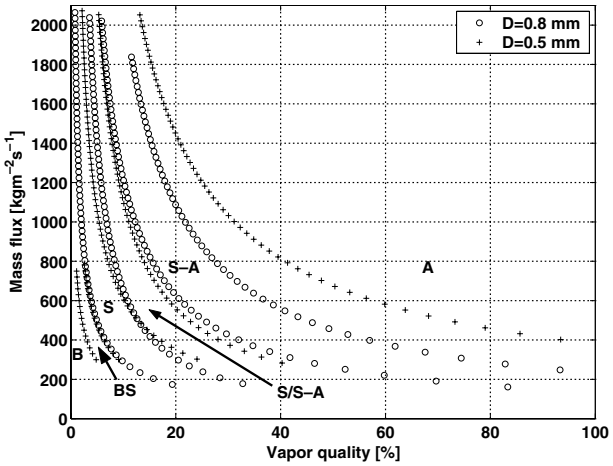

Fig. 12. Comparison between experimental transition lines from two different diameters from laser 1 for R-134a, $\Delta T_{sub} = 3$ °C, $T_{sat} = 30$ °C, $L = 70.70$ mm.

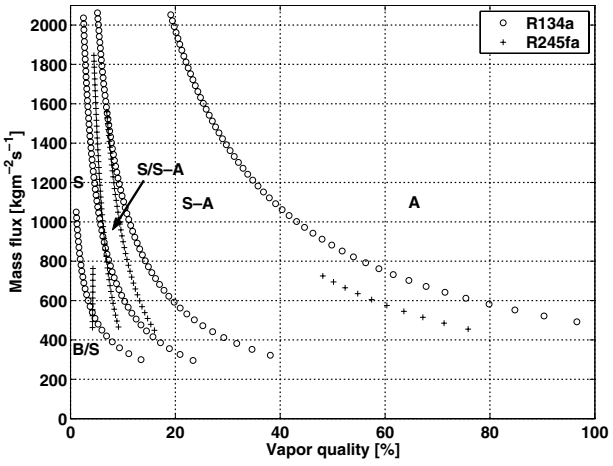

Fig. 13. Comparison between experimental transition lines from two different fluids from laser 1 for $D = 0.5$ mm, $T_{sat} = 35$ °C, $L = 70.70$ mm.

as above. Theoretically a longer tube with low heat flux at a given mass flux and vapor quality would result in longer bubbles at outlet of the heated tube. The transitions between flow regimes would probably appear earlier in terms of vapor quality.

The effect of the inside diameter is shown in Fig. 12. Bubbly flow for $D = 0.8$ mm would probably have been seen at the lower mass fluxes but the tests could not be run at those conditions due to instabilities in the heater. Bubbly/slug flow is present over a wider range of mass flux for the 0.8 mm tube. Except for the semi-annular/annular transition (for the same reasons explained earlier), no significant difference is observable in the locations of the transition lines. One may conclude that the two-phase mechanisms for the two different inside diameters are the same. For R-134a, 0.8 mm is still a microchannel based on the form of its experimental transition lines. A significant difference in the flow regime locations on the flow map could be a way to determine whether it is microscale or macroscale.

Fig. 13 presents the difference in the transition line locations between R-134a and R-245fa. The latter is a low pressure fluid (2.1 bar versus 8.9 bar of R-134a at 35 °C). To avoid a vacuum in the test section due to the high pressure drop with R-245fa, the tests were stopped when reaching the atmospheric pressure at the end of the evaporator and this is why annular flow was not reached at high mass flux. No bubbly flow was observed for the two fluids but it would probably have been seen at the lower mass fluxes but the tests could not be run at those conditions. One may observe that the transition lines tend to be more vertical for R-245fa than for R-134a, thus diverging at low mass fluxes, where the difference is significant and the flow regimes appear earlier in terms of vapor quality. However, the general trend of the transition lines remains the same and one may conclude that the two-phase flow transitions for R-245fa obey the same mechanisms as for R-134a.

5. Conclusions

An optical measurement method was used to characterize flow pattern transitions of two-phase flow in microtubes. It consists of shining two microlaser beams through a glass tube and the fluid at two different locations, using two lenses to focus the laser beams to the middle of the microtube, and using two photodiodes to recuperate the intensity of the light, whose signals are used to distinguish whether liquid, vapor, or liquid and vapor are present in the cross section. Bubble frequency, lengths of bubbles and flow pattern transitions are parameters that are able to be determined by this technique. Mean vapor velocity is also calculable from the measurements at some test conditions.

Four principal flow patterns (bubbly flow, slug flow, semi-annular flow and annular flow) with their transitions (bubbly/slug flow and slug/semi-annular flow) were observed in the present experiments with R-134a and R-245fa in 0.50 mm and 0.80 mm circular channels. Regime changes were detected by signal frequency analysis combined with a small bubble coalescence study. The higher the mass flux is, the earlier the transitions are encountered in terms of vapor quality. Bubbly flow tends to disappear at high mass flux because small bubbles quickly coalesce to form elongated ones.

Many observations have been made on the transitions between flow regimes. The two-phase flow pattern transitions observed with R-134a did not compare well to a leading macroscale flow map for refrigerants nor to a microscale map for air–water flows. No significant influence of the inlet subcooling nor the saturation pressure has been observed on the flow pattern transitions. A shorter heated length did not influence the locations of the transition lines. The diameter effect did not show any difference, although bubbly/slug flow is present over a wider range of mass flux. The transitions between flow regimes are less influenced by the mass flux for R-245fa

than for R-134a; However, the two-phase flow transitions for R-245fa are quite similar to those of R-134a.

Acknowledgements

Revellin is supported by the European Community's Human Potential Programme under contract HPRN-CT-2002-00204, [HMTMIC] funded by OFES, Bern, Switzerland and more recently by Swiss National Science Foundation (SFN) grant number 20 111626/1.

References

Cornwell, K., Kew, P.A., 1992. Boiling in small channels. In: Pilavachi, P. (Ed.), Proceedings of CEC Conference on Energy Efficiency in Process Technology. Elsevier, Athens, Greece, pp. 624–638.

Damianides, C.A., Westwater, J.M., 1988. Two-phase flow patterns in a compact heat exchanger and in small tubes. In: Proceedings 2nd UK National Conference On Heat Transfer, vol. 2, Glasgow, Scotland, pp. 1257–1268.

Dupont, V., Thome, J.R., Jacobi, A.M., 2004. Heat transfer model for evaporation in micochannels. Part 2: comparison with the database. Int. J. Heat Mass Transfer 47, 3387–3401.

Garimella, S., Killion, J.D., Coleman, J.W., 2002. An experimental validated model for two-phase pressure drop in the intermittent flow regime for circular channel. J. Fluid Eng. 124, 205–214.

Kasza, K.E., Didascalou, T., Wambsganss, M.W., 1997. Microscale flow visualization of nucleate boiling in small channels : mechanisms influencing heat transfer. In: Shah, R. (Ed.), Proceedings of International Conference on Compact Heat Exchangers for Process Industries. Begell House, New York, US, pp. 343–352.

Kattan, N., Thome, J.R., Favrat, D., 1998. Flow boiling in horizontal tubes: Part 1-Development of a diabatic two-phase flow pattern map. J. Heat Transfer 120, 140–147.

Lin, S., Kew, P.A., Cornwell, K., 1998. Two-phase flow regimes and heat transfer in small tubes and channels. In: Proceedings of 11th IHTC, Kyongju, Korea, vol. 2, pp. 45–50.

Lowe, D.C., Rezkallah, K.S., 1999. Flow regime identification in microgravity two-phase flows using void fraction signals. Int. J. Multiphase Flow 25, 433–457.

Mertz, R., Wein, A., Groll, M., 1996. Experimental investigation of flow boiling heat transfer in narrow channels. Calore e Tecnologia 14, 47–54.

Revellin, R., Dupont, V., Ursenbacher, T., Thome, J.R., Zun, I., 2006. Characterization of diabatic two-phase flows in microchannels: flow parameter results for R-134a in a 0.5 mm channel. Int. J. Multiphase Flow 32.

Saitoh, S., Daiguji, H., Hihara, E., 2005. Effect of tube diameter on boiling heat transfer of R-134a in horizontal small-diameter tubes. Int. J. Heat Mass Transfer 48, 4973–4984.

Serizawa, A., Feng, Z., Kawara, Z., 2002. Two-phase flow in microchannels. Exp. Thermal Fluid Sci. 26, 703–714.

Sheng, C.H., Palm, B., 2001. The visualization of boiling in small-diameter tubes. In: Heat Transport and Transport Phenomena in Microsystems, Banff.

Steinke, M.E., Kandlikar, S.G., 2003. Flow boiling and pressure drop in parallel flow microchannels. In: 1st International Conference on Microchannels and Minichannels, Rochester, US, pp. 1–12.

Suo, M., Griffith, P., 1964. Two-phase flow in capillary tubes. J. Basic Eng. 576–582.

Thome, J.R., Dupont, V., Jacobi, A.M., 2004. Heat transfer model for evaporation in micochannels. Part 1: presentation of the model. Int. J. Heat Mass Transfer 47, 3375–3385.

Triplett, K.A., Ghiaasiaan, S.M., Abdel-Khalik, S.I., Sadowski, D.L., 1999. Gas–liquid two-phase flow in microchannels part I : two-phase flow patterns. Int. J. Multiphase Flow 25, 377–394.

Wambsganss, M.W., France, D.M., Jendrzejczyk, J.A., Tran, T.N., 1993. Boiling heat transfer in a horizontal small-diameter tube. J. Heat Transfer 115, 963–972.

Yang, C.Y., Shieh, C.C., 2001. Flow pattern of air–water and two-phase R-134a in small circular tubes. Int. J. Multiphase Flow 27, 1163–1177.

Yun, R., Kim, Y., 2004. Flow regimes for horizontal two-phase flow of CO_2 in a heated narrow rectangular channel. Int. J. Multiphase Flow 30, 1259–1270.